

- 4 -
**SIMPLE
RADIATION**

SOUND RADIATION FROM PLANAR BAFFLES

One of the more important and useful areas of investigation is to examine the theory behind sound radiation from sources in a plane. This type of source most closely approximates the radiation mechanism for loudspeakers, namely, flat baffle boxes. To a first order, a loudspeaker in a box is like a loudspeaker in an infinite baffle. This is true so long as the baffle on which the device is mounted is more than about two or three times the area of the driver. For smaller baffles, the situation is more like sound radiation from a cap in a sphere because the box edges are so close to the sound radiator. Diffraction effects at the box edges account are a factor and we will discuss these in later chapters. In this chapter we will develop the general theory that we will use in the analysis that we will pursue in later chapters.

4.1 Circular Disk

The usual approach to determining the sound radiation from a portion of a plane is to use the Rayleigh integral

$$P(r | r_0) = -i\rho ckv_0 \int_S g(r | r_0) dr \quad (4.1.1)$$

$S =$ the surface which contains the source

$g(r | r_0) =$ the Green's Function for an infinite plane

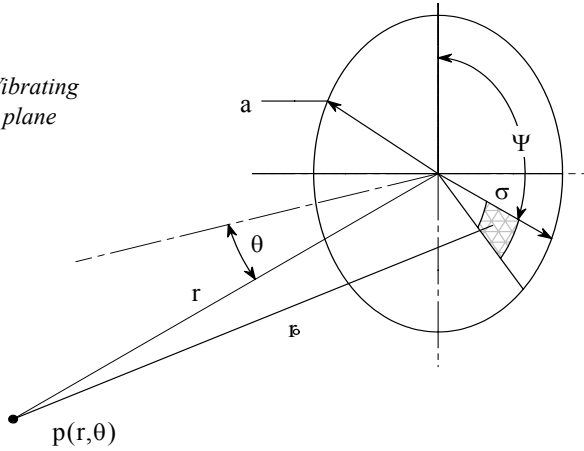
$v_0 =$ the velocity of the disk

The Green's Function in this case is simply twice the free space Green's Function that we introduced in the last chapter (a result of the perfectly reflecting plane)

$$g(r | r_0) = \frac{1}{2\pi} \frac{e^{ik|r-r_0|}}{|r-r_0|} \quad (4.1.2)$$

Curiously (or not), this is also the zero order Spherical Hankel Function. We shall see later that the Green's Function for polar geometries is, similarly, the zero order Hankel Function.

Figure 4-1 - Vibrating disk in a flat plane



As an example of the above procedure, consider the circular source shown above. Using Eq. (4.1.2) in Eq. (4.1.1) and noting that the only contribution to the integral comes from a circular region of the plane, we get

$$p(r, \theta) = \frac{i\rho c k e^{i k r}}{2\pi r} \int_0^{2\pi} \int_0^a v_0(\sigma, \psi) \sigma e^{i k \sigma \sin \theta \cos \psi} d\sigma d\psi \tag{4.1.3}$$

If the disk is a rigid piston, then v_0 is a constant and Eq. (4.1.3) becomes

$$p(r, \theta) = \frac{i\rho c k V_0 e^{i k r}}{2\pi r} \frac{2J_1(ka \sin \theta)}{ka \sin \theta} \tag{4.1.4}$$

$V_0 =$ the volume velocity (velocity times area) of the source

This result is a well known and the most widely used model for loudspeaker radiation. Unfortunately, it is hardly ever applicable. Fig. 4-2 shows the polar response map for a rigid piston as a function of ka .

Most transducers do not have radiating surfaces which are rigid pistons and so it would be convenient to generalize the approach shown above to consider non-rigid piston behavior. A convenient choice of modal description for the velocity distribution is given by

$$v_0(\sigma, \varphi) = \sum_{m,n} A_{mn} \cos(m \cdot \varphi) J_m \left(\frac{\beta_{mn} \sigma}{a} \right) \tag{4.1.5}$$

where β_{mn} are solutions of the equation

$$\left. \frac{d}{dx} J_m(x) = 0 \right|_{x=\beta_{mn}}$$

and are given in Table 4.1, "Eigenvalues for circular disk," on page 74 and Fig. 4-3 shows several of the radial modes ($m=0$) as defined by the above equations

Inserting Eq. (4.1.5) into Eq. (4.1.3) and rewriting the equation yields

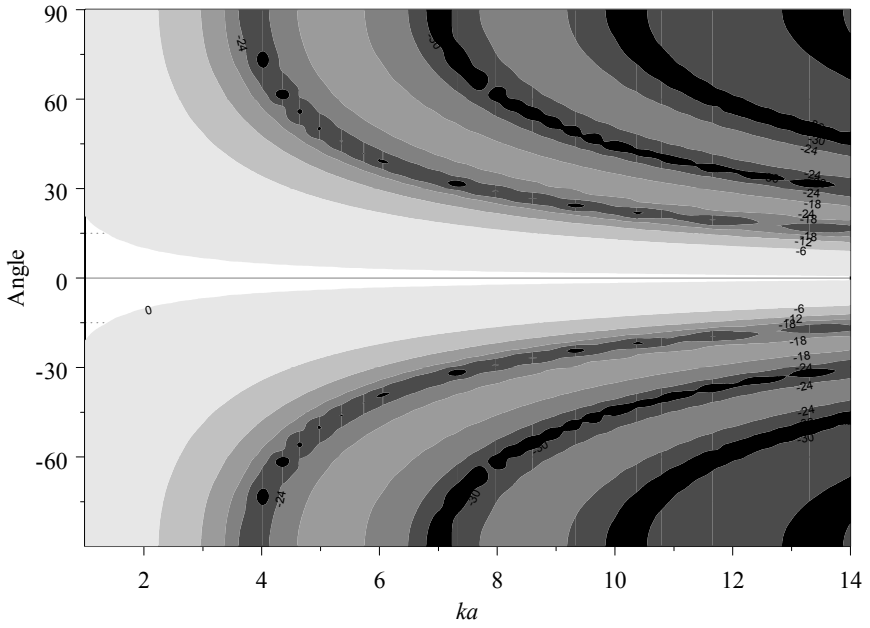


Figure 4-2 - Polar response map for a rigid piston

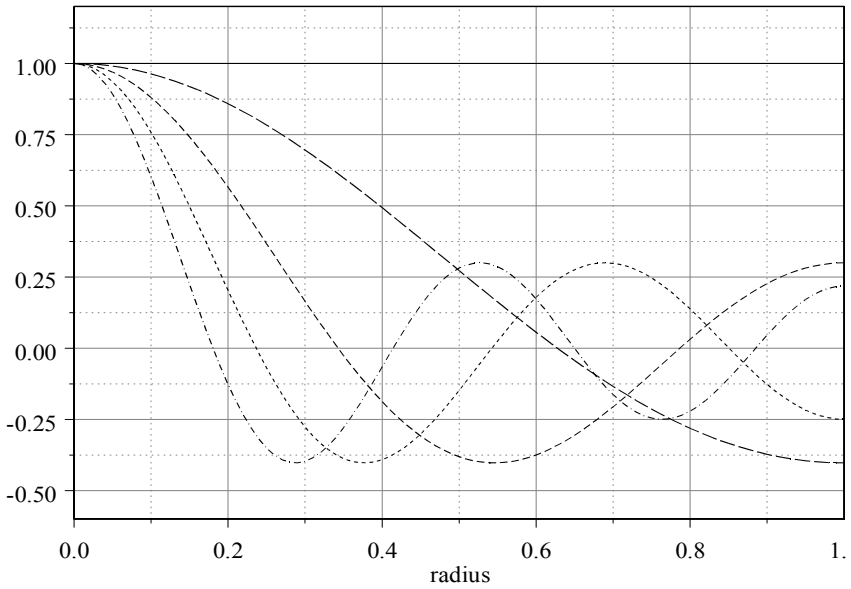


Figure 4-3 - Modal shapes for aperture velocity profiles in the radial direction

β_{mn}	n=0	1	2	3	4	5	6
m=0	0.0	3.8327	7.0152	10.1734	13.3238	16.4706	19.6158
1	1.8413	5.3313	8.5263	11.7059	14.8635		
2	3.0543	6.7060	9.9695	13.1705	16.3476		

Table 4.1: Eigenvalues for circular disk

$$p(r, \theta, \psi) \cong \frac{i\rho c k e^{i k r}}{2\pi r} \sum_{m,n} A_{mn} \cos(m\psi) \int_0^{2\pi} \int_0^a \cos(m\varphi) J_m\left(\frac{\beta_{mn}\sigma}{a}\right) \sigma e^{i k \sigma \sin\theta \cos\varphi} d\sigma d\varphi \tag{4.1.6}$$

where we have added a $\cos(m\varphi)$ term since axi-symmetry is not assumed here (as it was in the earlier equations). The approximation is required since the field point must be many wavelengths from the source, i.e. this equation is not valid in the near field. While this equation can be used directly in the form shown above, it is impractical and unnecessary.

Considering first the equation for φ we have

$$\int_0^{2\pi} \cos(m\varphi) e^{i k \sigma \sin\theta \cos\varphi} d\varphi = 2\pi i^m J_m(k\sigma \sin\theta) \tag{4.1.7}$$

Eq.(4.1.6) then becomes

$$p(r, \theta, \psi) = \frac{\rho c k e^{i k r}}{r} \sum_{m,n} i^{m+1} A_{mn} \int_0^a J_m(k\sigma \sin\theta) J_m\left(\frac{\beta_{mn}\sigma}{a}\right) \sigma d\sigma \cos(m\psi) \tag{4.1.8}$$

Using know relationships for the Bessel Functions and some significant offline algebra, we can reduce Eq.(4.1.8) to

$$p(r, \theta, \psi) = \frac{\rho c k S_0 e^{i k r}}{r} \sum_{m,n} i^{m+1} A_{mn} \Theta_{mn}(\theta) \tag{4.1.9}$$

$$\Theta_{mn}(\theta) = \frac{s(J_{m+1}(s) - J_{m-1}(s))}{(s^2 - \beta_{mn}^2)} \tag{4.1.10}$$

$S_0 =$ the area of the disk

$s = k a \sin\theta$

This is an important result for it shows that there are sound radiation modes for a circular planar baffled source just as there are for spherical and cylindrical baffled sources. Each vibration mode has its own characteristic radiation mode. This means that the sound radiation field can be decomposed into its “modal” response just as a membrane can. We will use this characteristic to significant advantage in Chap. 12.

The result shown here is not the most general case. The modal pattern of the source being analyzed must be describable by a cosine function, which is almost always the case when one can choose the location of the angular origin. In the completely general case, one simply has to add to the above formulation terms with a $\sin(\theta)$ variation. The analysis is identical and the results completely predictable, so they will not be discussed.

One last step needs to be shown. The coefficients A_{mn} need to be determined. From Eq.(4.1.5), and the power of orthogonality, these coefficients can be readily determined to be

$$A_{mn} = \frac{1}{\pi a^2} \int_0^{2\pi} \int_0^a v_0(\sigma, \psi) \cos(m\psi) J_m \left(\beta_{mn} \frac{\sigma}{a} \right) \sigma d\sigma d\psi \quad (4.1.11)$$

4.2 Examples of Circular Aperture Radiation

The above result can be greatly simplified for the case where the source is axisymmetric but still not a rigid piston – by far the most common situation. In this case there is no φ variation and the integer m must be zero, which reduces the results to

$$\Theta_n(\theta) = \frac{2sJ_1(s)}{s^2 - \beta_{0n}^2} \quad (4.2.12)$$

This form can be seen to reduce to the polar term found in Eq.(4.1.4) for a rigid piston. These functions, shown in Fig.4-4, have some interesting features. Note that for each modal function there is some value of $s = ka \sin(\theta)$ for which this mode is the only contributor. For example, at $s = 3.83$ the only mode which contributes to the response is the $n = 1$ mode. All other modes are zero. This means that for a source of radius .2 m operating at 2 kHz the pressure response at

$$\theta = \sin^{-1} \left(\frac{3.83}{2\pi \cdot 2000 \text{ Hz} \cdot .2 \text{ m}} \cdot 343 \text{ m/s} \right) = 31.5^\circ$$

results from the modal contribution of only the first mode. Note also that below about $ka = 2$, only the average velocity across the disk, i.e. the zero order mode, contributes to the response. This is why it is impossible to control the polar radiation response of a baffled source at low frequencies, there is only a single degree of freedom.

As a further example of the usefulness of the modal approach to source radiation, consider the radiation response of a spherical wavefront impinging on a circular aperture. In analyzing the sound radiation from the mouth of a waveguide, we can use this approach as a good approximation to the velocity distribution in the mouth aperture if the waveguide is terminated in a flat baffle. (Many researchers have used a piston model for this problem, which, as we shall see, is highly erroneous.)

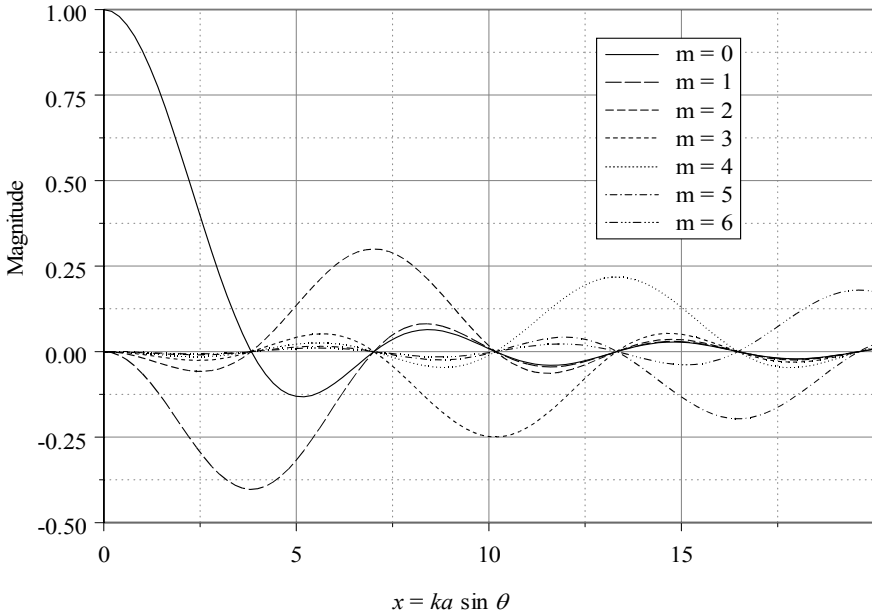


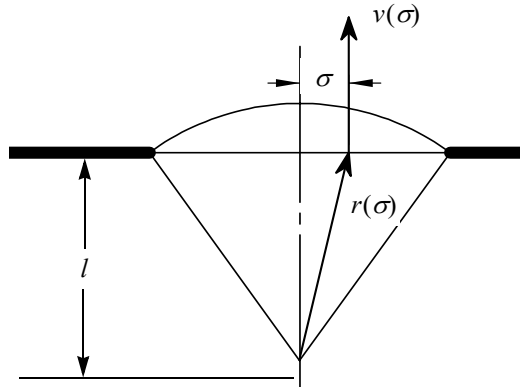
Figure 4-4 - Radiation modal functions of order n - circular case

Consider the drawing shown in Fig.4-5. We will use this model to calculate the modal representation of a spherical wavefront in an aperture. First, the problem is axi-symmetric so $m = 0$. The normal velocity $v(\sigma)$ within the aperture will vary with σ as $r(\sigma)$ according to

$$v(\sigma) = v_0 \frac{l^2}{l^2 + \sigma^2} e^{ik(\sqrt{\sigma^2 + l^2} - l)} \tag{4.2.13}$$

The magnitude and phase for the normal velocity at values of $ka = 1$ and $ka = 3$ are shown in Fig.4-6. Note that the magnitude is independent of frequency but

Figure 4-5 - Geometry for a spherical wavefront in a flat baffle



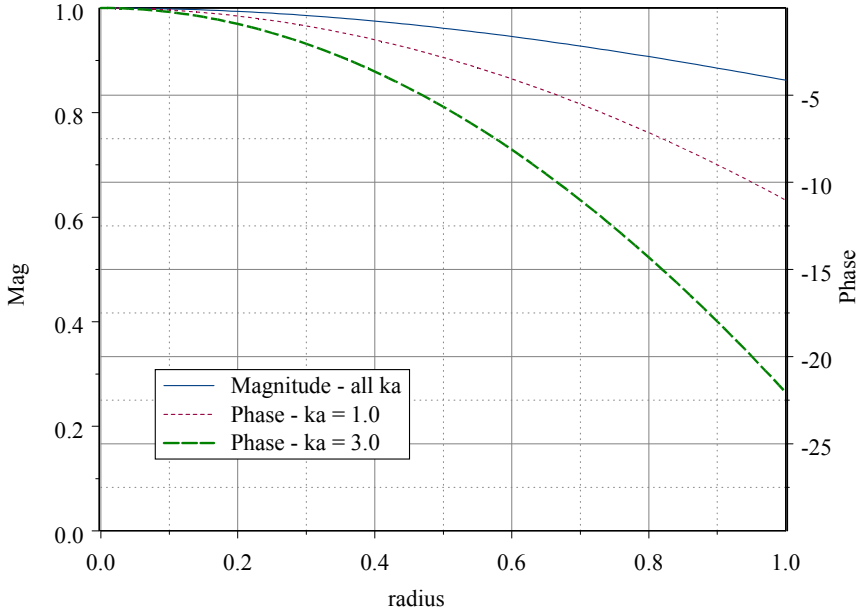


Figure 4-6 - Normal velocity magnitude (left) and phase for a spherical wavefront in an aperture

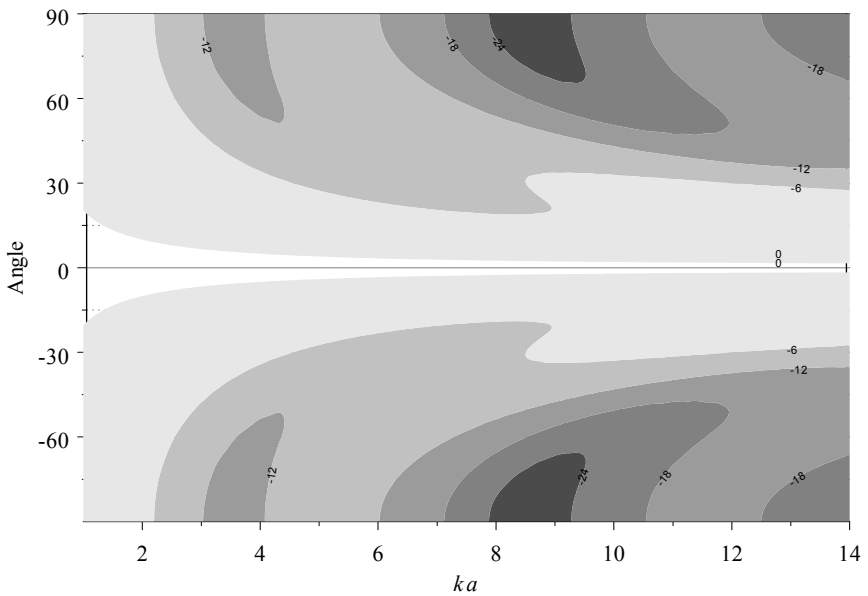


Figure 4-7 - The polar response map for a spherical wavefront

the phase is not. There is more phase shift at higher frequencies meaning that there is more of an effect on the polar response due to the spherical spreading of the wavefront.

The modal velocities can be calculated as

$$A_n(k) = \int_0^a \int_0^{\sqrt{a^2 - l^2}} (l^2 + \sigma^2)^{-1} e^{ik(\sqrt{\sigma^2 + l^2} - l)} J_0(\beta_{0n} \sigma/a) \sigma d\sigma \tag{4.2.14}$$

The polar response map of a spherical wave in the aperture is shown in Fig.4-7. When compared with the polar response of a plane wave (Fig.4-2 on page 73) in the same aperture it is clear that the directivity of a spherical wavefront is significantly different from that of a plane wave. Only at low frequencies ($ka < 4$) is the plane wave even remotely an accurate approximation to the spherical one.

4.3 The Rectangular Aperture As a Transform Pair

The next problem that we shall take up is that of a rectangular aperture as shown in Fig.4-8. The best way to describe the polar radiation for a rectangle is with two polar angles which we will call θ_x and θ_y . The rectangle will have dimensions $2a$ by $2b$. The far field radiation for this geometry is a simple extension of that which we have already been discussing

$$p(r, \theta_x, \theta_y) = i\rho c k \frac{e^{ikr}}{2\pi r} \int_{-\infty}^{\infty} \int_{-\infty}^{\infty} v_\omega(x, y) e^{ik_x x} e^{ik_y y} dx dy \tag{4.3.15}$$

$$k_x = k \sin \theta_x$$

$$k_y = k \sin \theta_y$$

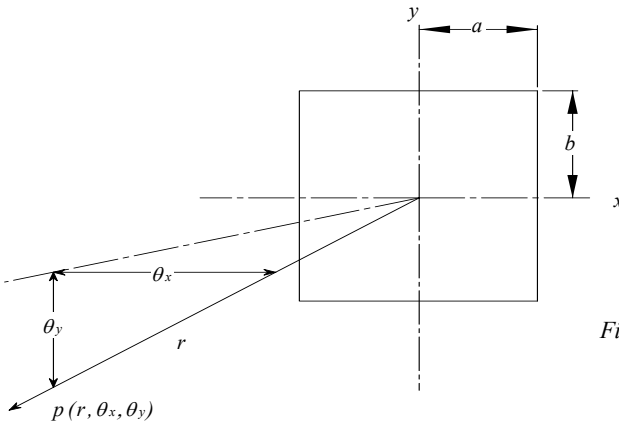


Figure 4-8 - Geometry for a rectangular aperture

We can at once recognize the double integral as a two-dimensional Fourier Transform in k -space. This result is quite interesting because it leads to several further observations. The first is that if the far field polar pattern is a Fourier Transform of the velocity profile in the plane then it must be that the inverse Fourier Transform of the far field polar pattern must then be the velocity distribution in the plane of the aperture. This concept is similar to the widely known theory of Nearfield Acoustic Holography (NAH) wherein one maps from the nearfield pressure response back to the velocity distribution in the plane or to the far field radiation pattern. The fundamental difference is that with NAH one also considers the so-called near field evanescent waves which do not propagate to the far field. This adds a significant complexity to the calculations but does allow for a greater resolution of the velocity distribution of the source.

Based on what we have learned thus far we should realize that we could actually draw a desired polar map and take the inverse transform to find the velocity distribution that would achieve that response. There is no guarantee that this distribution is either finite or realizable, however, which is another subject altogether. We will see an example of how we might get around this limitation in Chap.6.

Another aspect of this transform relationship is that all of the properties of the Fourier Transform that we know (and love) are applicable. For instance if a complex source can be broken down into a convolution of simple sources then the polar pattern is simply the product of the polar patterns for the individual sources. For example, consider two square identical pistons spaced apart by a constant d along the x axis as shown in Fig.4-9. The resulting polar pattern would simply be the product of the polar pattern of a bipole (two in phase point sources separated by a small displacement), $\cos(kd \sin \theta_x)$, and the polar pattern of a single square piston (which we will derive shortly). This generalized transform result is also known as the *First Theorem of Sound Radiation*. Whenever one of the sources being convolved is a point source then the convolution is particularly simple to perform. However, the power of this technique is applicable to much more complicated relationships.

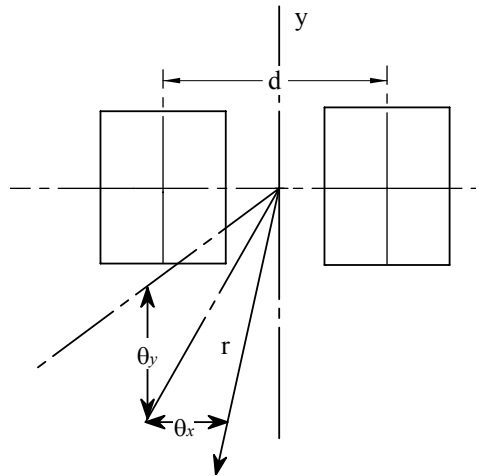


Figure 4-9 - Geometry for dual source example

Another aspect of the transform relationship between source velocity and sound radiation involves the multiplication of the velocity profile by some useful function. For example, we will want to know the effect of smoothing the velocity

function, such as when the mouth of a waveguide is flared into the baffle (as opposed to a discontinuous termination wherein the velocity profile drops abruptly to zero). This effect can be approximated by multiplying (or convolving) the velocity function at a discontinuous mouth by a Gaussian function e^{-ax^2} where a sets the width of the curve – basically the inverse of the width of the aperture. The reason that the Gaussian function is so convenient is that its Fourier Transform is also a Gaussian function. The polar response then becomes the convolution (or multiplication) of the abruptly terminated mouth response with a Gaussian function. The result acts to smooth the spatial ripples in the polar response, which resulted from the diffraction of the wavefront at the discontinuous mouth. There is no end to the interesting features that one can glean from the transform relationship between the velocity and the far field response.

Lastly, we could easily just ignore one of the spatial dimensions in which case we would have the polar pattern for a planar baffled line source with elements whose width is much less than the length of the line. All of the properties described above would hold including the fact that the shading (variable drive voltages for the elements in the line) is simply the inverse transform of the desired vertical polar pattern.

4.4 Generalized Rectangular Radiation

We will now solve the problem of radiation from a rectangular aperture in the general case. The velocity profile is first expanded as a two dimensional function

$$F(x, y) = A_n \cos\left(n\pi \frac{x}{a}\right) \cdot B_m \cos\left(m\pi \frac{y}{b}\right) \tag{4.4.16}$$

Not all rectangular velocity profiles can be represented by this equation but for the most part any profile that we are likely to come across can be so represented or certainly approximately so.

Inserting Eq.(4.4.16) into Eq.(4.3.15) we get

$$\begin{aligned} p(r, \theta_x, \theta_y) &= i\rho ck \frac{e^{jkr}}{2\pi r} \sum_{n,m} A_n B_m \int_{-b}^b \int_{-a}^a \cos\left(n\pi \frac{x}{a}\right) \cos\left(m\pi \frac{y}{b}\right) e^{ik_x x} e^{ik_y y} dx dy \\ &= i\rho cka^2 \frac{e^{jkr}}{2\pi r} \sum_{n,m} A_n B_m G_n(ka \sin \theta_x) \cdot G_m(kb \sin \theta_y) \end{aligned} \tag{4.4.17}$$

where

$$G_n(x) = (-1)^n \frac{x \sin(x)}{(x)^2 - (n\pi)^2} \tag{4.4.18}$$

Note that G_0 is a Sinc function.

Of course the coefficients A_n and B_m have to be determined, but by now that should be obvious

$$A_n = \int_{-a}^a v(x) \cos\left(n\pi \frac{x}{a}\right) dx$$

$$B_m = \int_{-b}^b v(y) \cos\left(m\pi \frac{y}{b}\right) dy$$
(4.4.19)

As we said before, we have assumed that the velocity profile can be decomposed into a product of separate profiles in x and y .

We should take a few lines to talk about the functions $G_m(\theta)$. Fig. 4-10 shows a plot of the first five values of m as a function of $x = ka \sin \theta$. The similarity of these functions to the functions of Sec. 4.2 (see Fig. 4-4 on page.76) is striking, although we should have anticipated this since there is very little difference between the two derivations. The fact that the functions, all except one, cross the zero point at the same point is an important feature which is identical between these functions and those in the previous section. The characteristics described therein would thus be the same.

Fig. 4-11 shows a polar map of the zero order mode (top) and the first order mode (bottom). These maps bear a strong resemblance to those for a circular aperture.

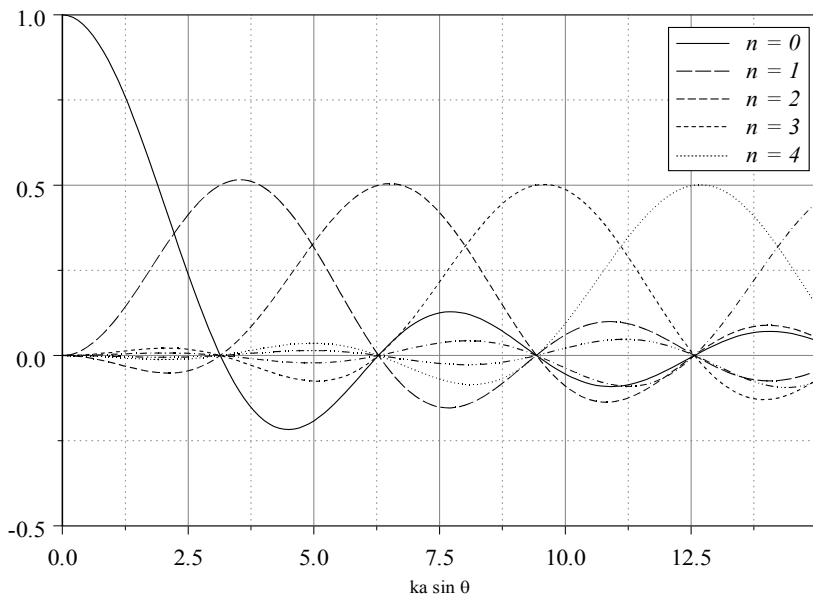


Figure 4-10 - First five rectangular modal functions

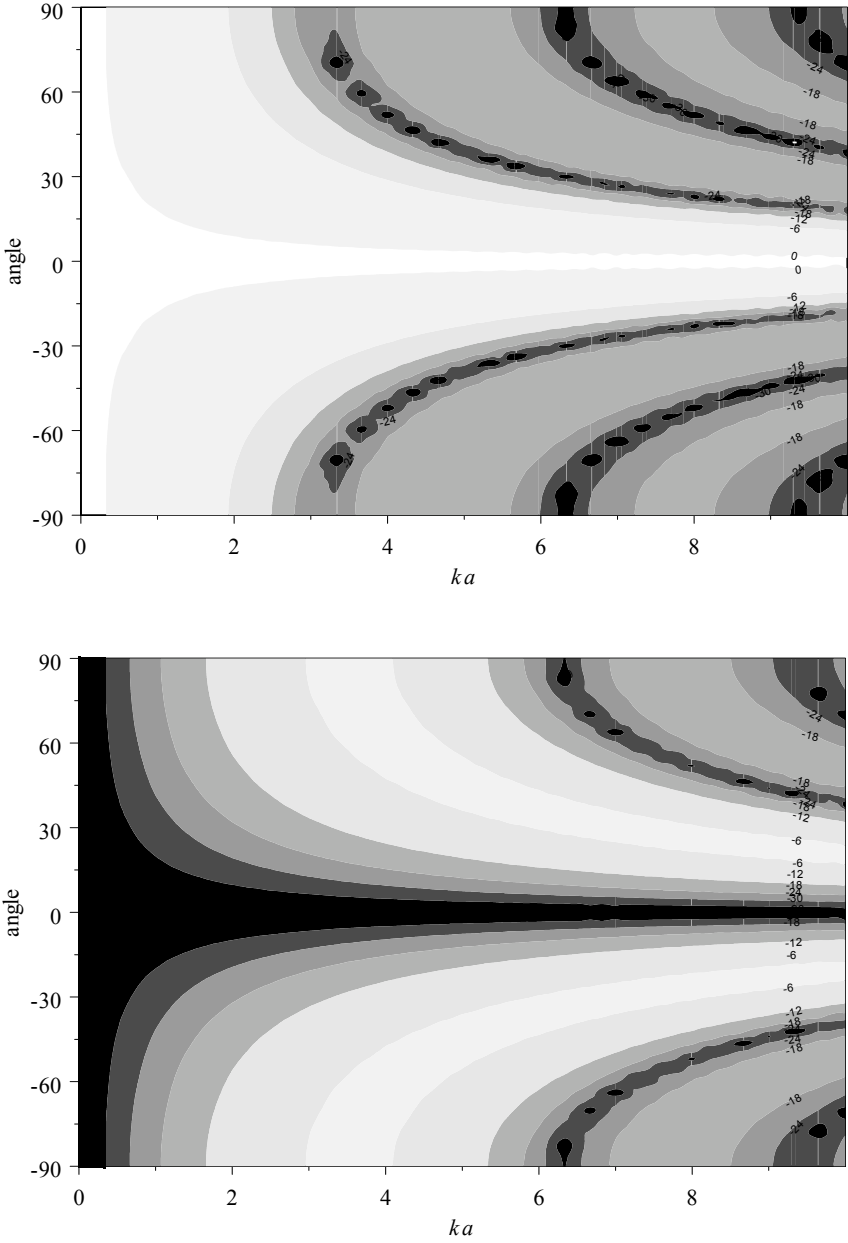


Figure 4-11 - Polar response for Rectangular polar modes, $n=0$ (top), $n=1$ (bottom)

4.5 Transform Relationships for Circular Apertures

By now we should expect that the circular aperture will also have a transform relationship. This transform is called the *modified finite Hankel Transform*. (“*modified finite*” because it is applied to an orthogonal set of finite Bessel Functions of the form shown in Fig 4-4). This set and the expansion of a circular aperture constitutes what is called a *Fourier–Bessel series*.

The Hankel Transform pair are

$$H_{n\alpha} \{F(\sigma)\} = \int_0^\infty F(\sigma) \sigma J_n(\alpha\sigma) d\sigma = f_H(\alpha) \quad (4.5.20)$$

$$H_{n\sigma} \{f_H(\alpha)\} = \int_0^\infty f_H(\alpha) \alpha J_n(\alpha\sigma) d\alpha = F(\sigma)$$

Among the elegance of these equations is the fact that the forward and inverse transforms are identical. Special properties of the Hankel Transform, for the $n=0$, case are shown in Table 4.2. For our problems $\alpha = ka \sin \theta$. The first three pairs

	$F(\sigma)$	$f_H(\alpha)$
1	$\frac{1}{\sigma} J_0\left(\frac{c}{\sigma}\right)$	$\frac{1}{\alpha} J_0(2\sqrt{c\alpha})$
2	$\begin{cases} 1 & \text{if } 0 < \sigma < c \\ 0 & \text{if } \sigma > c \end{cases}$	$\frac{c}{\alpha} J_1(c\alpha)$
3	$\int_0^\infty y G(y) \int_0^\pi F\left(\sqrt{x^2 + y^2 - 2xy \cos \theta}\right) d\theta dy$	$\pi f_H(\alpha) g_H(\alpha)$
4	$\frac{1}{c^2} F\left(\frac{\sigma}{c}\right)$	$f_H(c\alpha)$
5	$\frac{1}{\sigma}$	$\frac{1}{\alpha}$
6	$e^{-c\sigma}$	$c(\alpha^2 + c^2)^{-\frac{1}{2}}$

Table 4.2: Hankel Transform pairs

are fundamental properties and the second three are more specific, but interesting examples. Property 3 is in fact the convolution integral form of the Hankel Transform – a circular convolution. It can be quite useful, as we shall see. Property 2 could be quite useful.

As an example, consider a waveguide constructed as an annular ring source with an annular horn. Sources like this have been available in the marketplace. We can approximate this configuration as a source with an outer radius a and an inner radius b (property 2 used twice), which are circularly convolved (property 3) with a Gaussian (property 6) to approximate the spherical spreading.

$$V(\sigma) = \int_a^b y \int_0^\pi e^{c\sqrt{\sigma^2+y^2-\sigma y \cos\theta}} d\theta dy \tag{4.5.21}$$

The function $V(\sigma)$ is shown in the figure below.

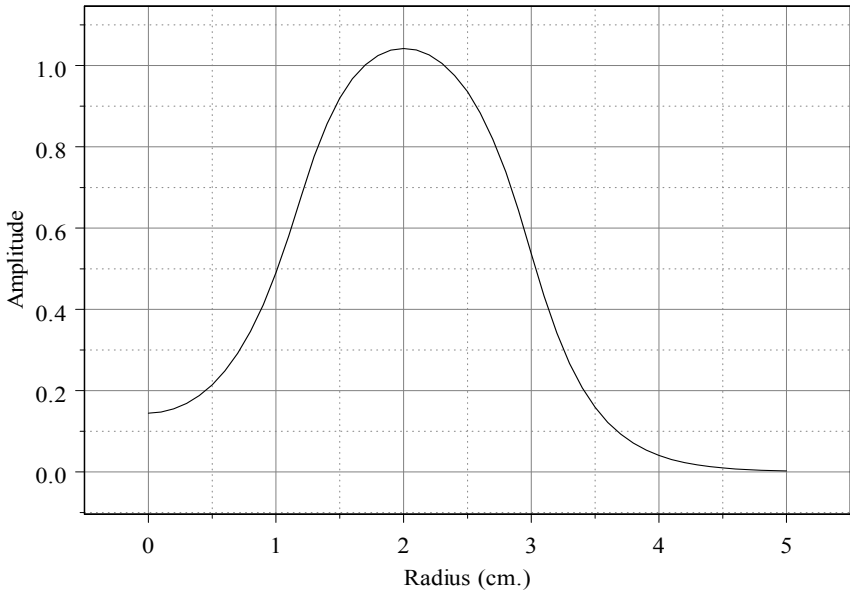


Figure 4-12 - The velocity distribution for the annular waveguide example

From the above table we can see immediately that the radiation pattern is simply the difference in two sources of radius a and b multiplied by the polar pattern for a Gaussian

$$\left(\frac{a}{\alpha} J_1(a\alpha) - \frac{b}{\alpha} J_1(b\alpha) \right) \cdot \frac{c}{\sqrt{\alpha^2 + c^2}} \tag{4.5.22}$$

The variable c is chosen to fit the velocity distribution to the aperture. In our example we will use $a=.012$, $b=.03$ and $c=300$. The polar map for this velocity

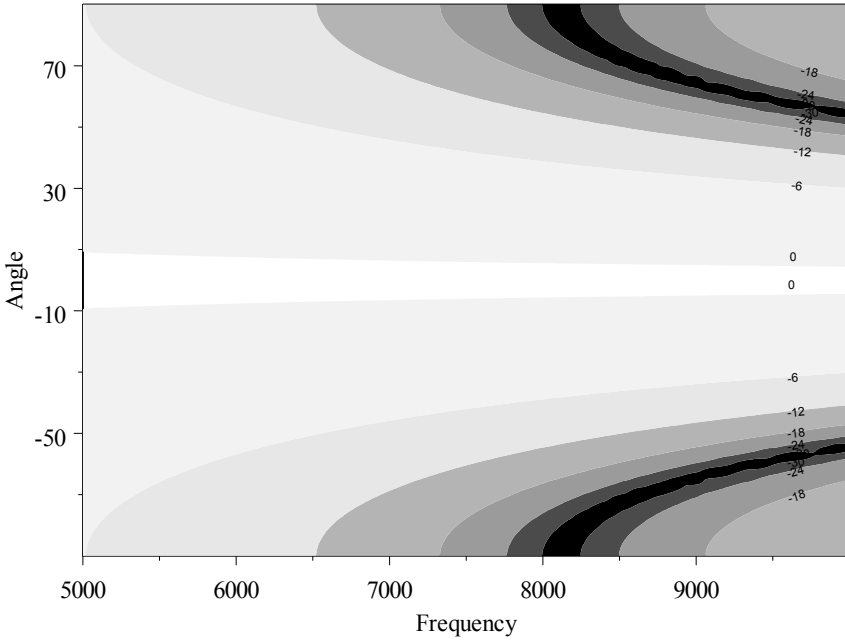


Figure 4-13 - Polar response map for an shaded annular ring

distribution is shown in Fig.4-13. Clearly the transform method offers a simple technique for calculating the polar response for this type of source.

4.6 Non-planar Sources in a Flat baffle

We will now investigate the problem of a non-planar source located behind the baffle. We have the tools to find the radiation response from any velocity distribution in the plane of the baffle, but a source which is not coincident with the baffle (i.e. a flat piston) will not have a velocity distribution in the aperture which is flat. If we use the three dimensional Green's Function

$$\frac{e^{ikR}}{2\pi R} \tag{4.6.23}$$

where R is shown in Fig.4-14. The source element $dx d\theta$ has θ as its angular location, which is not evident is the cross sectional drawing. A study of this figure shows that

$$R(\sigma, x, \theta) = \sqrt{h^2 - 2\frac{h^2 x}{b} + \sigma^2 + x^2 - 2\frac{\sigma x}{b} \sqrt{(b^2 - h^2) \cos(\theta)}} \tag{4.6.24}$$

We can now determine the velocity distribution $v(\sigma)$ in the baffle plane from

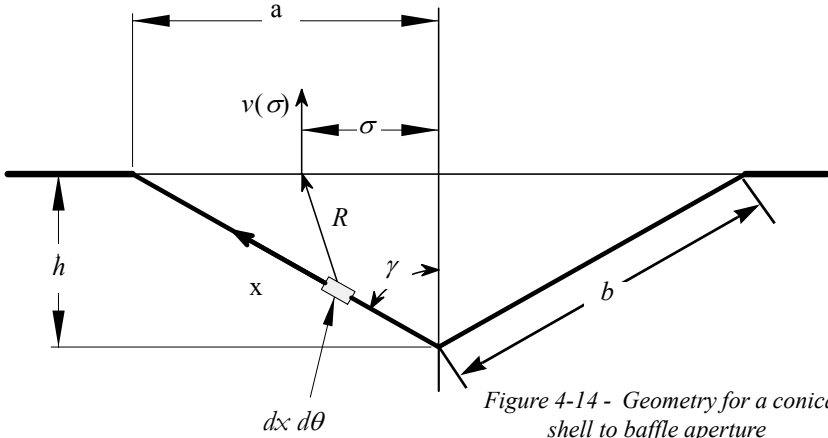


Figure 4-14 - Geometry for a conical shell to baffle aperture

$$v(\sigma) = \frac{1}{\pi \sin(\gamma)} \int_0^b \int_0^\pi v_0(x, \theta) \frac{e^{ikR(\sigma, x, \theta)}}{R(\sigma, x, \theta)} x d\theta dx \tag{4.6.25}$$

$v_0(x, \theta)$ = normal velocity at each point on cone.

We should note that this approach is only approximately correct. The exact approach¹ considers the actual impedance in the baffle plane and the acoustical resonances which occur in the cavity. These later effects can be significant, but are not accounted for in Eq.(4.6.25). None the less, this equation does give us an indication of the effect that a cavity has on the directivity response function with far less calculation than the exact result requires. From Porter, we know that there is a slight rise in the response due to a cavity resonance of very low Q at a ka value which depends on the cavity volume. It is about 3 dB at $ka = 1.8$ for a small cavity (like that shown in Fig.4-14) and about 6 dB at $ka = 2$ for a larger volume. At ka value above about 4, there are severe dips in the response due to standing waves across the aperture that have a zero net velocity. These later effects cannot be accounted for with the method shown here, but the former effect can be simulated with a small gain added to the zeroth order radiation mode. This correction is not used here.

Fig.4-15 shows the velocity distribution in the plane of the aperture for $ka = 1, 3$ and 5. The velocity tends to focus at the center of the aperture, an effect which is consistent with Porter.

These velocity distributions can be decomposed into their modal contributions from Eq.(4.1.11) with $m = 0$

1. See Porter, et.al. "A Boundary Element Approach", *JAES*

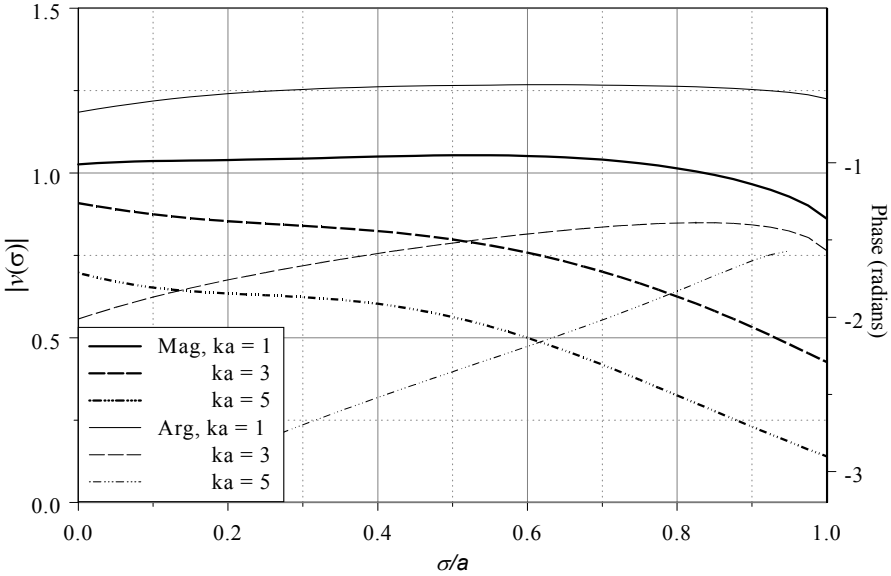


Figure 4-15 - Velocity distribution in the plane of the aperture

$$A_n(ka) = \frac{1}{a} \int_0^a v(ka, \sigma) J_0 \left(\beta_{0,n} \frac{\sigma}{a} \right) \sigma d\sigma \tag{4.6.26}$$

where the Bessel Functions are defined on page 73. The A_n 's calculated from this equation are shown in Fig.4-16. The zero mode, the average velocity, is seen to fall off with ka as the aperture velocity becomes more non-planar. The higher order modes above the third can be seen to be negligible, but the first and second mode rise, which will tend to broaden the directivity pattern. The polar response map for a concave cone is shown in the top half of Fig.4-17. The bottom half of this figure is the flat piston source. The cone does not have a significantly wider directivity although the depth of the off axis null has been modified greatly.

4.7 Summary

This chapter has shown how one can analyze the polar response pattern from virtually any source in a baffle. We have ignored the effect of a finite baffle, since it is our belief that one should minimize the diffraction from baffle edges, thus making their effect negligible. We will discuss this more in later chapters. Important applications to the sound radiation problem, a spherical wavefront and a concave source were shown to be tractable with our techniques.

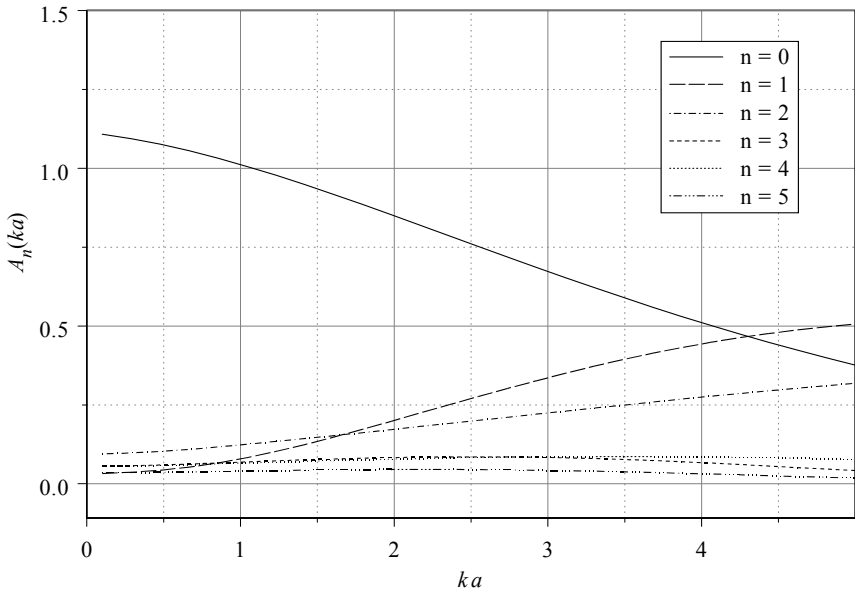


Figure 4-16 - Modal velocity contributions

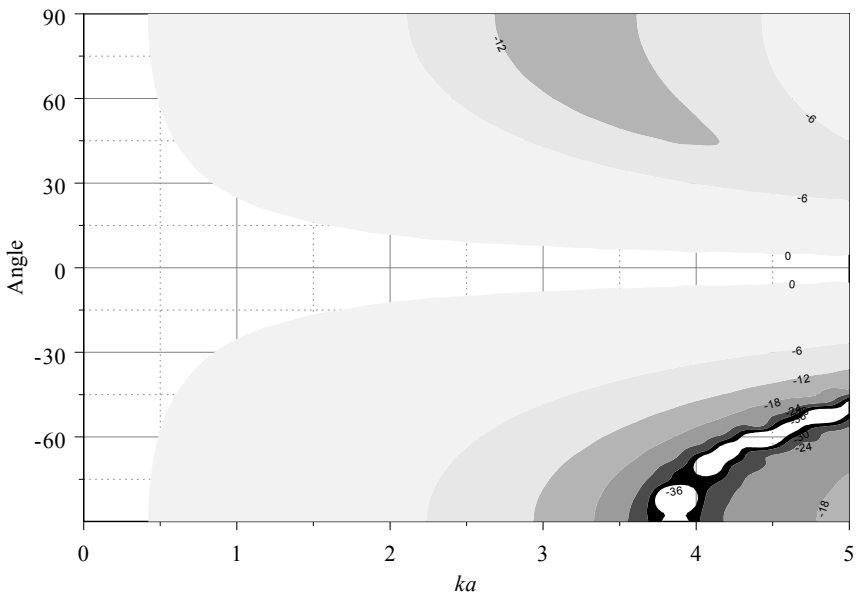


Figure 4-17 - Polar response map for concave cone (top) and flat piston